Metallophysics and Advanced Technologies
Металофіз. новітні технол.
Metallofiz. Noveishie Tekhnol.
2026, vol. 48, No. 4, pp. 367–382
https://doi.org/10.15407/mfint.48.04.0367
Reprints available directly from the publisher

PACS numbers: 61.43.Dq, 61.72.Dd, 61.72.Ff, 62.20.fg, 65.60.+a, 81.05.Bx, 81.30.Kf

Structure and Properties of Heat-Treated $(TiHf)_{50}(NiCu)_{50}$ Alloys

N. A. Gurbanov[*], H. A. Ahlatci[**], K. H. Ismayilova[*], and Y. A. Abdulazimova[***]

[*]*Azerbaijan State Oil and Industry University,*
16/21 Azadlig Ave.,
AZ-1010 Baku, Azerbaijan
[**]*Karabük University,*
Kılavuzlar, 413. Sokak No: 10.,
TR-78050 Merkez/Karabük, Turkey
[***]*Baku Engineering University,*
120 Hasan Aliyev Ave.,
AZ-0101 Khirdalan, Azerbaijan

Shape-memory alloys are metallic smart materials, which can recover their original shape after deformation and primarily consist of two main solid phases. This study develops physical principles for selecting chemical compositions for quaternary alloys with shape-memory effects and other functional properties obtained using conventional and unconventional technologies. Studies on the $(TiHf)_{50}(NiCu)_{50}$ system obtained by rapid cooling have revealed that amorphous–crystalline or completely amorphous phases can form, depending on the composition. Furthermore, it is determined that the martensitic-transformation temperature, which depends on copper concentration in the alloys, does not change in rapidly cooled strip samples.

Key words: shape-memory alloy, sheet metal, planar flow casting, amorphous structure, enthalpy of mixing.

Стопи з пам'яттю форми — це металеві «розумні» матеріяли, які можуть відновлювати свою початкову форму після деформації та переважно

Corresponding author: Nurlan Gurbanov
E-mail: nurlan.gurbanov@asoiu.edu.az

Citation: N. A. Gurbanov, H. A. Ahlatci, K. H. Ismayilova, and Y. A. Abdulazimova, Structure and Properties of Heat-Treated $(TiHf)_{50}(NiCu)_{50}$ Alloys, *Metallofiz. Noveishie Tekhnol.*, **48**, No. 4: 367–382 (2026), DOI: 10.15407/mfint.48.04.0367

складаються з двох основних твердих фаз. У цьому дослідженні розроблено фізичні принципи вибору хемічного складу для чотирокомпонентних стопів з ефектами пам'яті форми й іншими функціональними властивостями, одержаними за допомогою традиційних і нетрадиційних технологій. Дослідження системи $(TiHf)_{50}(NiCu)_{50}$, одержаної швидким охолодженням, показали, що, залежно від складу, можуть утворюватися аморфно-кристалічні або повністю аморфні фази. Крім того, було встановлено, що температура мартенситного перетворення, яка залежить від концентрації Купруму у стопах, не змінюється у швидкоохолоджених зразках стрічки.

Ключові слова: стоп з пам'яттю форми, листовий метал, лиття планарним потоком, аморфна структура, ентальпія змішання.

(Received 18 November, 2025; in final version, 15 December, 2025)

1. INTRODUCTION

Today, technology is rapidly evolving to meet increasing needs. This rapidly advancing technology brings with it new generations of materials and instruments.

In addition to the physical properties of materials, different types of materials with different functionalities have been developed today [1]. High functionality can be achieved by controlling and monitoring the micro-level movements of smart materials, which are products of advanced technology, and by changing their internal structures in response to environmental effects [2, 3]. One of the most functional structures among smart metals is the shape-memory alloy [4]. Shape-memory alloys are defined by the ability of the material to return to its original shape, usually by heating, after severe deformations that occur at relatively low temperatures [3, 5, 6]. The shape-memory effect in shape-memory alloys is due largely to the solid–solid diffusionless thermoelastic martensitic transformation between cubic $B2$ austenite and monoclinic $B19'$ martensite phases [4, 7].

How $B2$ austenite transforms into $B19'$ martensite and how twinning occurs during the martensitic transformation, it has been investigated using atomistic simulations [8]. It is observed that when martensite grains nucleate within austenite, they form a twin relationship as a natural consequence of the crystal structure (Fig. 1). Atomic mixing is all that is required for the lattice transformation and twinning, and since the twinning plane cannot be kept fixed during the lattice transformation, no homogeneous slip occurs on the twinning plane. In this case, the twinning mechanism does not involve dislocations, and it is possible to achieve thermoelastic martensitic transformation.

The thermoelasticity of the transformation arises from the material's ability to elastically accommodate the stresses caused by the

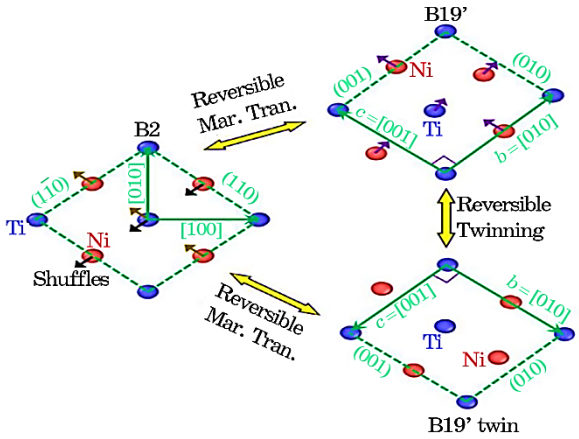

Fig. 1. Lattice transformations between *B*2, *B*19', and mirrored *B*19' [8].

volume change during the crystallographic rearrangement of different phases [5, 8]. As a general rule, the volume effect during thermoelastic martensitic transformation is very small (< 1%), which allows the consistency of the austenite/martensite interfaces to be maintained during the transformation [9]. The kinetic parameters of the thermoelastic martensitic transformation in shape-memory alloys can be followed by different kinetic models [10]. Common models for the simultaneous study of martensitic transformation are the Flynn–Wall–Ozawa and Kissinger models. The Kissinger approach determines a specific activation energy and thermal activation required for the transformation as a result of the effect of the heating/cooling rate on the reaction [4, 11]. The Ozawa approach is very similar to the Kissinger approach except that the reaction order is not affected by the heating/cooling rate [12].

Nanoscale precipitates are used in shape-memory alloys to tailor thermoelastic martensitic transformations [13]. These precipitates significantly affect the thermoelastic martensitic-transformation properties by introducing concentration heterogeneity, coherent stress field and geometric confinement in the parent phase [1, 14].

Among the shape-memory alloys, NiTi alloys stand out due to their good functional and mechanical properties such as ductility, fatigue strength, deformation rate [8, 9]. Today, NiTi alloys constitute the majority of shape-memory alloys used practically in industry, especially in biomedical fields [11]. However, since the transformation temperatures of NiTi alloys are below 100°C, their use is limited in areas requiring high temperatures such as aerospace, automobile and petroleum industries [15]. Therefore, researchers are working on developing materials with transformation temperatures above 100°C [16]. The most important alloy systems emphasized in the studies are the mate-

rials obtained by increasing the transformation temperatures of these alloys by alloying and precipitation formation methods using the NiTi binary alloy system as a base [17, 18]. Thus, the good properties of Ni-Ti alloys are utilized and alloys that can exhibit phase transformation at high temperatures can be obtained [19, 20]. One of the most important methods used for this purpose is alloying [16].

When combining NiTi binary alloys with a third alloying element, both the transformation temperatures of these alloys can be increased and some mechanical properties can be improved [4, 12–14]. With the changes made, it has been observed that the transformation temperatures of the elements V, Fe, Al, Mn, Cu, and Co added as third alloying elements decrease, while the phase transformation temperatures of Hf, Zr, Pt, Au, and Pd increase [15, 21]. Because Au, Pt, and Pd are very expensive, among these elements, which increase the phase-transformation temperatures, researchers have focused mostly on Hf and Zr [2, 4, 9]. Among these two elements, it has been determined that Hf is more preferred than Zr in terms of ductility, work production capacity, and cost [12–15, 21]. Moreover, the phase transformation temperatures of NiTiHf alloys can be adjusted between 100–300°C. The transformation temperatures of NiTiHf alloys do not increase negligibly up to 10% Hf content. However, it increases rapidly after 10% Hf addition and when the Hf ratio is 30%, the phase transformation temperatures continue above 500°C [9, 21].

The main disadvantages of NiTiHf alloys with low Ni content can be listed as low ductility, high thermal hysteresis (> 50°C) and low strength. Various studies have been carried out to increase the strength of these alloys [22]. One of these is to increase the strength by means of high deformation and the dislocations formed in the microstructure as a result [23]. As a result of these studies, it has been observed that the reversible deformation obtained increases and the thermal hysteresis values decrease [21–23]. Another method for improving the properties of NiTiHf alloys is precipitation hardening. This method is one of the methods that have been successful in increasing the strength. Studies have increased the strength and improved the functional properties of NiTiHf alloys by precipitation hardening [24–25].

Kollerov *et al.* [26] investigated a titanium–nickelide alloy alloyed with up to 1% Co, Cr, and Fe, up to 3% V, and up to 8% Nb. Kolomytsev *et al.* [27] investigated the effects of Fe, Al, and Cu on phase transformations in TiNi alloys.

Most metallic materials used in practice are not in complete thermodynamic equilibrium, corresponding to the maximum free energy. Obtaining alloys in a metastable state is considered an effective approach to ensure their physicochemical properties [4, 10, 28]. It is known that upon cooling below the melting temperature (T_m), the alloy either

transforms into an amorphous state or crystallizes. When crystallization occurs, the viscosity, volume, and internal energy change abruptly. If crystallization can be prevented, these properties change continuously and rapidly with temperature [2, 10, 14]. The crystallization kinetics of amorphous alloys is determined by the combined effects of thermodynamic factors and kinetic parameters [28–31].

Research has shown that the strengthening of the TiNi compound cannot be achieved sufficiently by alloying alone [16, 20–25].

This work offers a thorough thermodynamic–structural correlation for the quaternary $(TiHf)_{50}(NiCu)_{50}$ system created by planar flow casting under rapid cooling, in contrast to earlier research that focused exclusively on NiTiHf or NiTiCu systems. This study is noteworthy in that it demonstrates how differences in the enthalpy of mixing and amorphous phase stability produced by copper influence the behaviour of the martensitic transition following rapid quenching. Furthermore, the study develops a new framework for forecasting amorphous–crystalline transitions in multicomponent Ti-based shape-memory alloys by fusing theoretical modelling of mixing enthalpies (Ni–Ti *vs.* Ni–Hf subsystems) with actual calorimetry. For (TiHf)–(NiCu) systems, the dual thermodynamic–kinetic methodology allows for a quantifiable relationship between alloy composition, enthalpy landscape, and structural state evolution that has not before been demonstrated in the literature. As a result, the findings contribute to the development of high-temperature shape-memory materials with tuneable martensitic-transformation temperatures above the NiTiHf threshold and adjustable amorphous stability.

2. RESEARCH METHODOLOGY

2.1. Technology of Obtaining Layers as a Result of Ultra-Fast Cooling

For the preparation of the studied alloys, titanium (Ti), hafnium (Hf), nickel (Ni) and copper (Cu) chemical elements with a purity of 99.9–99.99% are used. The alloys are prepared by the induction method (the total weight of the casting varies from 30 g to 60 g).

For ultra-fast cooling, the ‘master’ alloys given in Table 1 were used. The samples were prepared by the planar casting method. In this method, the distance between the rapidly moving mass disk and the liquid metal is stable (less than 1 mm; in our alloys, this distance was 0.15–0.2 mm). The hole, into which the liquid metal is poured, is of 0.3–0.35 mm, and its length is of 7–10 mm. These distances allow the cross-section of the obtained ribbons to be large. A 5–15 g section of the mentioned ‘master’ alloy is placed in a quartz tube and heated by the induction method. The temperature is controlled by pyrometers. The temperature of pouring the alloy onto the casting drum is taken

TABLE 1. Nominal chemical composition, alloy heat treatment temperature $T_{\text{heat treat.}}$ [°C] and symbols of the studied samples.

Alloy symbol	Alloy composition, at.%	$T_{\text{heat treat.}}$, °C
SMA (1.1)	$Ti_{32}Hf_{18}Ni_{50}$	1300
SMA (1.2)	$Ti_{32}Hf_{18}Ni_{45}Cu_5$	1280
SMA (1.3)	$Ti_{32}Hf_{18}Ni_{35}Cu_{15}$	1220
SMA (1.4)	$Ti_{32}Hf_{18}Ni_{25}Cu_{25}$	1220

50–150 K above the liquidus line, while the viscosity of the alloy is also taken into account. The pouring process is carried out in an argon atmosphere under a pressure of 0.2 MPa. The material of the disk onto which the alloy is poured is made of Cu (Co–Be), and its diameter is of 200 mm. The rotation speed of the disk is between 5–30 m/s (optimal speed of 19 m/s, pressure of 0.2 MPa) (Fig. 2).

Heat Treatment of Samples. A tubular vacuum furnace was used for heat treatment of samples. This furnace belongs to the class of electric resistance furnaces and allows full temperature control. For complete thermal stabilization of samples, they are placed in a package (two parallel steel sheets).

The heat treatment process combines the following sequence: cut strips (flakes) are collected in a special package and placed in the middle of a quartz tube. With the help of a forevacuum pump, the pressure is brought to 10^{-2} torr, and with the use of a turbomolecular pump, to 10^{-5}. After that, the thermal treatment mode is set: heating rate, temperature, holding time (at a specified temperature) and the cooling process of the package.

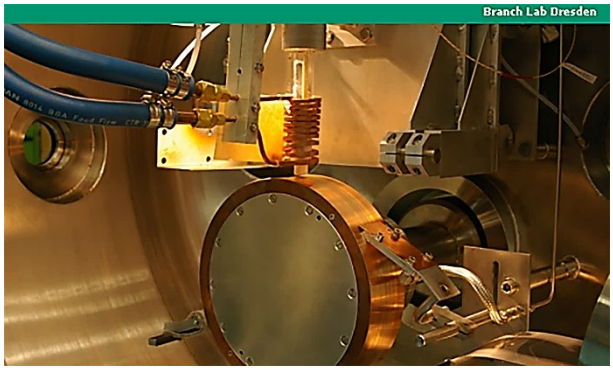

Fig. 2. The device used to produce ultra-fast hardened layers operates using the planar casting method.

The heating rate can be set to 300 K/h and 600 K/h, the isothermal holding mode can be set in the range of 300–900°C from 2 minutes to 4 hours, cooling is carried out in air. At this point, the sample package is removed from the quartz tube (and the quartz tube is cooled in a vacuum, as mentioned).

After the heat treatment process, the structure of the alloys was systematically studied using x-ray diffraction analysis, electron microscopy, and calorimetric methods.

X-Ray Diffraction Analysis. X-ray diffraction analysis was performed on a Philips diffractometer using CuK_α radiation (CoK_α) (voltage of 40 kV, current of 30 mA). The 20 angle was determined between 10–90°.

Transmission Electron Microscopy (TEM). A JEOL 1220 JEM transmission electron microscope (TEM) was used to determine the structure and phase boundaries of the samples.

Differential Scanning Calorimetry (DSC). Differential scanning calorimetry was used to study accurately any phase transformations that depend on temperature.

3. RESULTS AND DISCUSSION

3.1. Formation Enthalpy of Liquid Alloys of the $(TiHf)_{50}(NiCu)_{50}$ System

The heat of formation of liquid alloys of the two-component systems Ni–Ti and Ni–Hf was studied by the calorimetric method at 1873 K. The experiment consisted in continuously adding a certain mass of refractory metals and recording the thermal effect of their dissolution.

Several experiments were conducted for each system to study the enthalpies of mixing of refractory metals with nickel. It was found that the indicators of each of them were the same, and then they were processed together. The method of approximation of the experimental results consisted in constructing a simple polynomial model to describe the concentration dependence of the function of αMe partial enthalpy of mixing. The optimal degree of the polynomial was determined using the Fisher statistical criterion. Then, by integrating the dependence obtained according to the Gibbs–Duhem equation, the concentration dependence of the partial property of the second component and the integral enthalpy of mixing were calculated. It was carried out at a value of 0.95 for all quantities (amounts).

The phase diagrams of the studied system [32–34] show that in the crystalline state there is a strong interaction between the particles of the components, which determines the presence of a significant number of intermetallic compounds in them: three for the Ni–Ti system, eight for the Ni–Hf one. In addition, the thermal stability (stability or durability or strength) of the more difficult to melt of them is comparable to the thermal stability of pure nickel. The similar picture of the

phase diagrams [20, 22, 25] allows us to assume that a significant negative deviation from ideality should be observed for alloys of this system. The conducted experimental studies and the analysis of the literature data on the thermodynamic properties of alloys [21, 23, 30, 34, 35] have proven this assumption.

Ni–Ti System. The partial mixing enthalpies of titanium with nickel have been determined in the composition interval $x_{Ti} = 0–0.6$. The partial enthalpies of mixing titanium with nickel are more exothermic quantities. We have been able to express their concentration dependence by the following equation, kC/mol:

$$\Delta\overline{H}_{Ti} = \left(1 - x_{Ti}\right)^2 \left(\begin{array}{l} -194.90 - 151.54x_{Ti} - 1313.49x_{Ti}^2 + 18937.67x_{Ti}^3 - 43418.87x_{Ti}^4 + \\ +29329.04x_{Ti}^5 \end{array} \right).$$

The first minimum enthalpy of mixing of titanium is –194.9±11.0 kC/mol. This value is in complete agreement with the value at 1873 K (–185.0±8.0 kC/mol) in Ref. [36].

The integral enthalpy of mixing of the components is expressed as concentration dependence, kC/mol:

$$\Delta H = x_{Ti}\left(1 - x_{Ti}\right) \left(\begin{array}{l} -194.89 - 74.16x_{Ti} - 462.33x_{Ti}^2 + 4710.12x_{Ti}^3 - \\ -8881.36x_{Ti}^4 + 5010.65x_{Ti}^5 \end{array} \right).$$

The minimum integral enthalpy of mixing is at $x_{Ti} = 0.37$: 41.6±1.1 kC/mol. The enthalpies of mixing obtained in Refs. [19, 33] at 1741 and 1838 K, respectively, agree with our results within the experimental error. However, the results of Refs. [22, 36] show a higher exothermic value at 2000 K. In our opinion, such a picture does not correctly reflect the nature of the temperature dependence of the enthalpy of mixing in the Ni–Ti system, but rather indicates the inaccuracy of individual experimental studies.

Ni–Hf System. The concentration dependence of the enthalpy of mixing for the Ni–Hf system was also studied. For this purpose, two experiments were conducted with $x_{Hf} = 0–0.48$. The equation for the concentration dependence of the enthalpy of mixing of Hf, kC/mol, is as follows:

$$\Delta\overline{H}_{Hf} = \left(1 - x_{Hf}\right)^2 \left(\begin{array}{l} -246.43 + 352.33x_{Hf} - 5630.42x_{Hf}^2 + 322107.21x_{Hf}^3 - \\ -59429.21x_{Hf}^4 + 34285.09x_{Hf}^5 \end{array} \right).$$

The enthalpy of mixing of hafnium at infinite dilution is of –244.4±10.4 kC/mol. According to the results of the studies, the first enthalpy of mixing of hafnium was calculated at 1873 K and the value was determined to be of –214.0±10.0 kC/mol.

The following equation was derived to express the concentration

dependence of the integral enthalpy of mixing in the Ni–Hf system, kC/mol:

$$\Delta H = x_{\text{Hf}}\left(1 - x_{\text{Hf}}\right)\begin{pmatrix} -244.21 + 88.04x_{\text{Hf}} - 942.52x_{\text{Hf}}^2 + 3951.07x_{\text{Hf}}^3 - \\ -3898.18x_{\text{Hf}}^4 \end{pmatrix}.$$

In the composition of hafnium $x_{\text{Hf}} = 0.1$, the integral enthalpy of mixing takes a minimum value of -49.6 ± 1.8 kC/mol.

The analysis of the conducted research and literature data [20–25] shows that the enthalpies of mixing in the Ni–Ti and Ni–Hf systems take anomalously large (for metal–metal type systems) exothermic values. When passing from titanium-containing alloys to hafnium-containing alloys, the magnitude of their exothermicity is observed. This regularity is confirmed for the first enthalpy of mixing of the components and the minimum values of the enthalpies of mixing.

It is obvious that the mentioned regularity is also reflected in the interaction of these elements in the crystalline state, which is expressed by the increase in the thermal stability of the intermetallic phases in this (Ni–Ti) → (Ni–Hf) system. The change in the energetic characteristic of alloy formation of the system and the electrochemical factor, which we used the phasor of the square of the electronegativities of the components, correlates with the change in its character.

The large difference between the electronegativities of the components, the high exothermic heat of their alloy formation, the finding of the minimum integral enthalpy of mixing in the density interval where the most difficult-to-melt intermetallics are present, allow us to speculate about the possibility of localization of chemical bonding in the studied metallic alloys and, as a result, the occurrence of structure-density diversity in the type of chemical combination in them.

A quantitatively similar (identical) hypothesis can be carried out by modelling the thermodynamic properties of alloys within the framework of the theory of associated ideal solutions.

It should be noted that the interest of researchers in the thermodynamic properties of alloys formed by nickel with Ti and Hf is primarily related to their high amorphous formation properties. Within the framework of experimental studies and the results of the proposed (applied) modelling, it can be assumed that the thermodynamic parameters of the alloy formation processes are such that the strong interaction of the components and the tendency of the alloy to form associates allow the alloy to become amorphous during rapid cooling.

3.2. Structure of Rapidly Quenched Alloys of the $(TiHf)_{50}(NiCu)_{50}$ System

As mentioned above, one of the main reasons for the formation of amorphous phases during rapid annealing of metallic alloys is the spe-

cific nature of the interaction between the components of liquid solutions. By studying the thermodynamic properties of amorphous formation systems, for example, the integral formation enthalpy of interparticle interaction of components in different aggregate states, we were able to determine the composition of the alloys [16–20, 22, 25, 37–39].

Although the total length of the layers for each alloy was 15–16 meters, the thickness varied depending on the annealing temperature and speed. 1 m was selected from the central part of the layer for the study, and each end of the part was examined by x-ray structural analysis. In order to clarify the difference between the parts close to the drum and free parts of the layers, the structure of both faces was studied. Then, the layers were cut into 20 cm lengths and checked for uniformity.

3.3. Structure of Rapidly Quenched $Ti_{32}Hf_{18}Ni_{50-x}Cu_x$ Alloys

The first series of $Ti_{32}Hf_{18}Ni_{50-x}Cu_x$ (x = 0, 5, 10, 15 and 25 at.%) alloys of the $(TiHf)_{50}(NiCu)_{50}$ system, which were quenched at high speed, were selected as the research object.

Initially, the rapidly quenched $Ti_{32}Hf_{18}Ni_{35}Cu_{15}$ alloy was investigated. Its x-ray structure was studied, and a diffractogram was recorded. The diffractogram was obtained using CoK_α radiation (Fig. 3). As seen in this figure, in the range of 2θ = 40–55°, a broad interference peak appears in the first coordination sphere. In the second coordination sphere, a weaker interference peak was identified in the range of 2θ = 70–85°. According to the literature, such spectra are characteristic of amorphous materials; however, in order to confirm with certainty that the alloy possesses an amorphous structure, it is also essential to examine its structure using electron microscopy.

For this purpose, the investigated $Ti_{32}Hf_{18}Ni_{35}Cu_{15}$ alloy was additionally studied by electron microscopy. The results of this investigation are presented in Fig. 4. As can be observed, the rapidly quenched

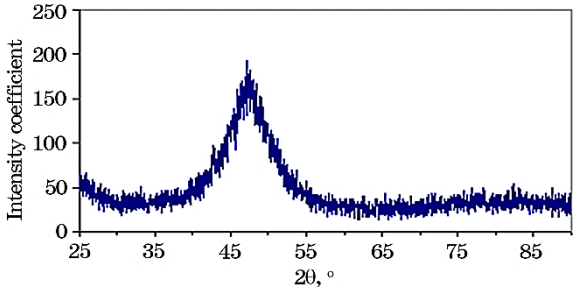

Fig. 3. Diffractogram of the initial state of the $Ti_{32}Hf_{18}Ni_{35}Cu_{15}$ alloy quenched at high speed. T = 20°C, free surface of the layer.

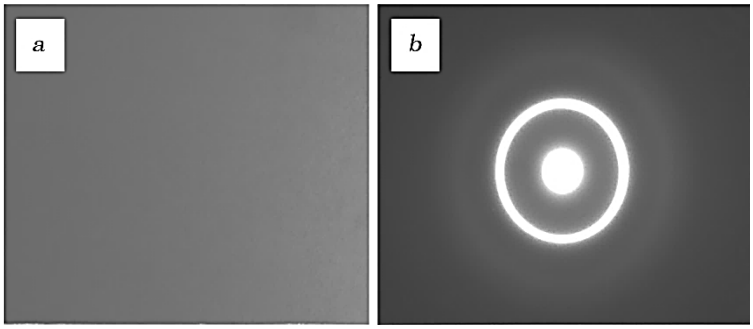

Fig. 4. Initial state image (*a*) and corresponding electron-diffraction pattern (*b*) of the high-speed quenched $Ti_{32}Hf_{18}Ni_{35}Cu_{15}$ alloy. $T = 20°C$, free surface of the layer.

$Ti_{32}Hf_{18}Ni_{35}Cu_{15}$ alloy has an amorphous structure (Fig. 4, *a*). The corresponding microelectron-diffraction pattern exhibits a diffraction halo, which provides further evidence of the amorphous structure.

Since the rapidly quenched $Ti_{32}Hf_{18}Ni_{45}Cu_5$ alloy was found to exhibit a different structure based on the initial results, its investigation was carried out using several additional methods. The x-ray structure of this alloy was studied over a wider range, and a diffractogram was obtained. The diffractogram was recorded using CoK_α radiation (Fig. 5). As seen in the figure, in the range of $2\theta = 40–55°$, a broad interference peak appears in the first co-ordination sphere; however, superimposed on this peak are lines characteristic of a crystalline structure. In the second co-ordination sphere, no interference peak was detected.

Table 2 lists the possible phases, which can be formed in the studied samples (NiTiHf and TiNiCu are taken as the base elements), the possible structure and lattice parameters, which can be formed in them. When the diffractogram shown in Fig. 5 is calculated to the corresponding crystal structure, the presence of two crystal structures was

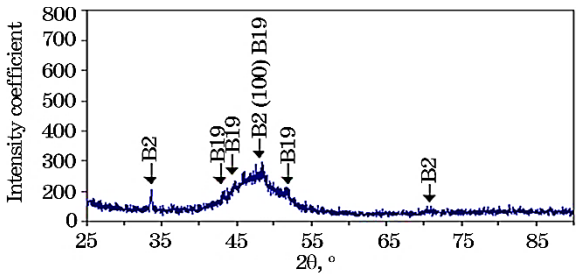

Fig. 5. Diffractogram of the initial state of the high-speed quenched $Ti_{32}Hf_{18}Ni_{45}Cu_5$ alloy. Free surface of the layer at $T = 20°C$.

TABLE 2. Possible phases that can be formed in the studied samples (NiTiHf and TiNiCu were taken as the base elements).

Alloy	Phase	Structure	Unit cell parameters
$Ni_{50}Ti_{32}Hf_{18}$	$B2$	CsCl type, b.c.c.	$a = 0.3075$nm
	$B19'$	monoclinic	$a = 0.304$, $b = 0.409$, $c = 0.438$, $\beta = 102.4°$
$Ti_{50}Ni_{50-x}Cu_x$	$B2$	CsCl type, b.c.c.	$a = 0.29$–0.31 nm
	$B19$	orthorhombic	$a = 0.29$, $b = 0.427$, $c = 0.451$ nm
	$B19'$	monoclinic	$a = 0.29$, $b = 0.40$, $c = 0.45$, $\beta = 100.2°$
NiTi, NiTiHf	Ti_2Ni		$a = 1.1324$ nm

TABLE 3. Calculation of the diffractogram of the initial state of the $Ti_{32}Hf_{18}Ni_{45}Cu_5$ alloy quenched at high speed. $T = 20°C$, free surface of the layer.

Line number	$d_{hkl\ \text{experimental}}$, nm	Identification
1	3.08931	$B2$ (100)
2	2.41858	$B19$ (101)
3	2.35371	$B19$ (002)
4	2.18244	$B2$ (110) + $B19$ (020,111)
5	2.05069	$B19$ (012)
6	1.54068	$B2$ (200)

revealed: $B2$ (CsCl type, b.c.c.) and $B19$ (martensite with orthorhombic crystal structure). All calculated parameters are given in Table 3.

The $Ti_{32}Hf_{18}Ni_{45}Cu_5$ alloy was also studied using a transmission electron microscope (TEM). Figure 6 shows the structure of the initial state (*a*–*c*) and the corresponding electron diffraction patterns (*d*–*e*) of the $Ti_{32}Hf_{18}Ni_{45}Cu_5$ alloy quenched at high speed. The thickness of the $B19$-martensite plates increases from $\cong 0.3$–0.4 μm (Fig. 6, *a*) to $\cong 0.75$ μm (Fig. 6, *b*). Figure 6, *b* shows a dislocation cluster in the martensite phase, such a structure is often found in crystal structures. Figure 6, *c* shows the self-assembly groups of the martensite plates. Figure 6, *d* shows the electron diffraction pattern corresponding to the (*a*) structure, and Fig. 6, *e* shows the electron diffraction pattern corresponding to the (*b*) structure. All images were taken at room temperature ($T = 20°C$), from the free surface of the layer. Images taken by an electron microscope show that the sample has an amorphous–crystalline structure.

Analogous results were obtained for the other two alloys studied: $Ti_{32}Hf_{18}Ni_{50}$ is amorphous-crystalline, and $Ti_{32}Hf_{18}Ni_{25}Cu_{25}$ alloy has an amorphous structure. All results, except for the characteristic temperatures of the martensite transformation after crystallization, are

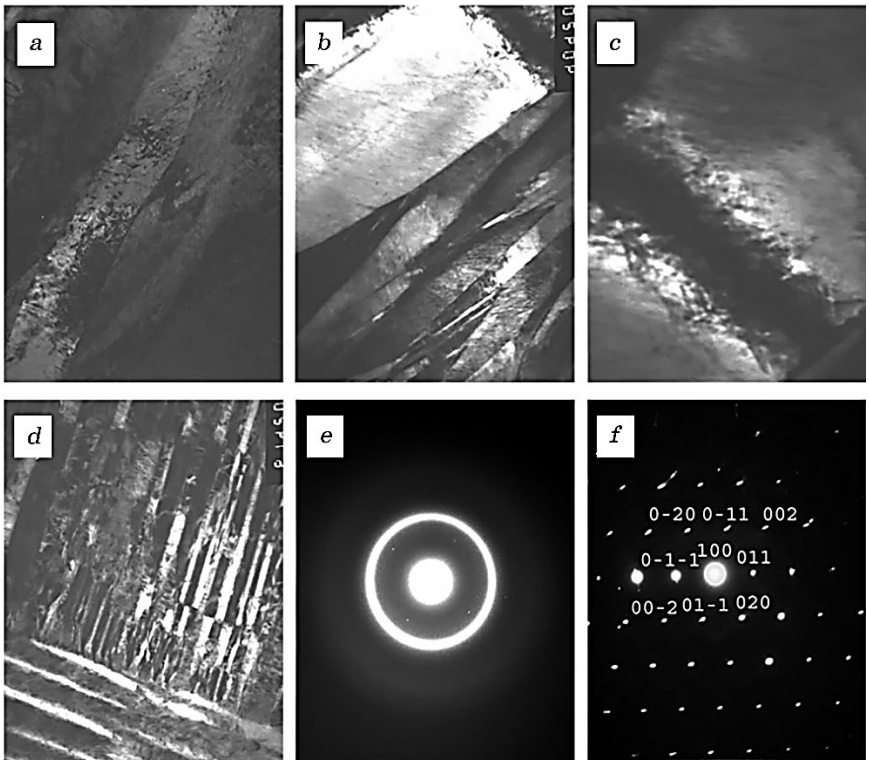

Fig. 6. Initial structure of the rapidly quenched $Ti_{32}Hf_{18}Ni_{45}Cu_5$ alloy (*a*–*c*) and the corresponding electron-diffraction patterns (*e*–*f*): (*a*) plates of *B*19 martensite (≅0.3–0.4 μm thick), (*b*) plates of *B*19 martensite (≅0.75 μm thick), (*c*) dislocation clusters in the martensitic phase, (*d*) self-accommodation groups of martensite plates, (*e*) electron-diffraction pattern corresponding to structure (*a*), (*f*) electron-diffraction pattern corresponding to structure (*b*). $T = 20$°C, free surface of the foil.

not presented in this paragraph, since they are completely repeated. In order to double-check the results of the studies, the phase transitions of $Ti_{32}Hf_{18}Ni_{50-x}Cu_x$ (x = 0, 5, 15, 25 at.%) alloys quenched at high speed were investigated in a calorimetric device.

All transformations occurring in alloys annealed at high speed with temperature changes are characterized by the graphical structure presented in Fig. 7. Figure 7 shows the calorimetric curve of the $Ti_{32}Hf_{18}Ni_{35}Cu_{15}$ alloy annealed at high speed (initial state, heating rate of 20 K/min). As can be seen from the figure, the layers with an amorphous structure have a number of special properties. Such properties can be better recorded by the calorimetric study method. When the sample is heated from $T = 200$°C to T_g (glass transition temperature), an exothermic reaction causes a small variation in the heat flux, which

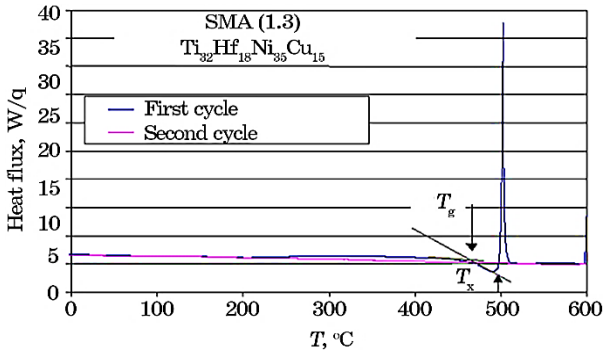

Fig. 7. Calorimetric curve of $Ti_{32}Hf_{18}Ni_{35}Cu_{15}$ alloy, high-speed annealing, heating rate of 20 K/min, initial state (first and second cycles).

in turn leads to structural relaxation in the amorphous phase.

The T_g parameter was determined to explain the temperature transition 'supercooled liquid–solid glass' in glasses and polymers. In our research objects, the T_g parameter is intended as a parameter indicating the approach of a supercooled liquid to a crystalline state in metallic amorphous alloys, a change in linear dependence. The T_x parameter is marked as the initial temperature of crystallization. As is known from the literature, at the beginning of crystallization, a smaller volume crystallizes (10^{-4}), and only then does total crystallization occur. The T_g and T_x temperatures depend on the heating rate, which, in turn, can be controlled by thermal analysis and calorimetry methods.

It is considered important to conduct heat treatment in high-speed hardened $Ti_{32}Hf_{18}Ni_{50-x}Cu_x$ (x = 0, 5, 15, 25 at.%) alloys to study the effect of structural changes on properties.

4. CONCLUSIONS

The following main results were obtained as a result of studying the structure and properties of high-speed quenched $(TiHf)_{50}(NiCu)_{50}$ alloys.

- The physical basis for the selection of chemical composition for four-component alloys with shape-memory effect and other functional properties, which can be obtained by traditional and unconventional technologies, has been developed. In alloys of the $(TiHf)_{50}(NiCu)_{50}$ system, which are annealed at high speed, it is possible to obtain different structural states depending on the composition: amorphous–crystalline or amorphous.
- The nature of the temperature dependence of the martensite transformation on the copper concentration in alloys of the $(TiHf)_{50}(NiCu)_{50}$ system does not change in layers obtained by depo-

sition from the liquid state.

In alloys of the $(TiHf)_{50}(NiCu)_{50}$ system, partial crystallization of the amorphous phase occurs (heating rate of 20 K/min) after thermal treatment in the T_g–T_x interval.

AUTHORS' CONTRIBUTIONS

K. H. Ismayilova performed the fabrication, heat treatment, and differential scanning calorimetry (DSC) analyses of the shape-memory alloy samples. Y. A. Abdulazimova conducted the x-ray diffraction (XRD) analyses to evaluate the integral mixture enthalpy of the constituent components. H. A. Ahlatci carried out the transmission electron microscopy (TEM) investigations and provided interpretation of the microstructural evolution. N. A. Gurbanov undertook the literature review, collected and analysed the experimental data obtained under laboratory conditions, and prepared the manuscript with input from all co-authors. All authors critically reviewed and approved the final version of the manuscript.

REFERENCES

1. Z. L. Wang and Z. C. Kang, *Functional and Smart Materials: Structural Evolution and Structure Analysis* (New York: Plenum Press: 1998).
2. W. Huang, *Materials & Design*, **23**, No. 1: 11 (2002).
3. L. Sun and W. Huang, *Metal Science and Heat Treatment*, **51**, No. 11: 573 (2009).
4. D. Hartl and D. Lagoudas, *Thermomechanical Characterization of Shape Memory Alloy Materials* (Springer–ABD: 2008).
5. K. Otsuka and X. Ren, *Intermetallics*, **7**, No. 5: 511 (1999).
6. G. Song, N. Ma, and H.-N. Li, *Engineering Structures*, **28**, No. 9: 1266 (2006).
7. A. Oudich and F. Thiebaud, *Mechanics of Materials*, **102**: 1 (2016).
8. B. Li, Y. Shen, and Qi. An, *Acta Mater.*, **199**: 240 (2020).
9. A. Shuitcev, R. N. Vasin, X. M. Fan, A. M. Balagurov, I. A. Bobrikov, L. Li, I. S. Golovin, and Y. I. Tong, *Scripta Materialia*, **178**: 67 (2020).
10. C. Ottavia, *Simulation Modelling Practice and Theory*, **11**: 5 (2003).
11. L. Yong, X. Zeliang, and J. V. Humbeeck, *Mater. Sci. Eng. A*, **273**: 673 (1999).
12. T.H. Grgurić, D. Manasijević, S. Kožuh, I. Ivanić, I. Anžel, B. Kosec, M. Bizjak, E. Govorčin Bajsić, Lj. Balanović, and M. Gojić, *J. Alloys and Compounds*, **765**: 664 (2018).
13. M. J. Jaronie, M. Leary, A. Subic, and M. A. Gibson, *Materials & Design*, **56**: 1078 (2014).
14. K. M. Knowles and D. A. Smith, *Acta Metall.*, **29**, Iss. 1: 101 (1981).
15. N. J. Aslanov, K. S. Mammadov, and N. A. Zeynalov, *IJATEE*, **9**, Iss. 87: 155 (2022).
16. K. Otsuka and X. Ren, *Prog. Mater. Sci.*, **50**, Iss. 5: 511 (2005).
17. J. Mohd Jani, M. Leary, A. Subic, and M. A. Gibson, *Mater. Des.*, **56**: 1078 (2014).

18. M. H. Elahinia, M. Hashemi, M. Tabesh, and S. B. Bhaduri, *Prog. Mater. Sci.*, **57**, Iss. 5: 911 (2012).
19. G. S. Firstov, H. J. Van, and Y. N. Koval, *J. Intell. Mater. Syst. Struct.*, **17**, Iss. 12: 1041 (2006).
20. H. E. Karaca, I. Kaya, H. Tobe, B. Basaran, M. Nagasako, R. Kainuma, and Y. Chumlyakov, *Mater. Sci. Eng. A*, **580**: 66 (2013).
21. J. Ma, I. Karaman, and R. D. Noebe, *Int. Mater. Rev.*, **55**, No. 5: 257 (2010).
22. X. L. Meng, W. Cai, L. M. Wang, Y. F. Zheng, L. C. Zhao, and L. M. Zhou, *Scr. Mater.*, **45**, Iss. 10: 1177 (2001).
23. R. K. Mehtiyev and Y. A. Tanriverdiyev, *J. Mach. Manuf. Reliab.*, **54**: 586 (2025).
24. I. S. Golovin and Y.X. Tong, *Scr. Mater.*, **178**: 67 (2020).
25. B. Kockar, I. Karaman, J. I. Kim, and Y. Chumlyakov, *Scr. Mater.*, **54**, Iss. 12: 2203 (2006).
26. M. Y. Kollerov, *Metals*, **5**: 53 (2007).
27. V. I. Kolomytsev and V. A. Lobodyuk, *Metallofizika*, **7**, No. 6: 36 (1985) (in Russian).
28. G. Pang, M. Jin, S. Zuo, and X. Jin, *Intermetallics*, **112**: 106527 (2019).
29. S. S. Mohammed, K. Mediha, I. N. Qader, and F. Dagdelen, *European Journal of Science and Technology*, **17**: 1014 (2019).
30. M. Y. Hasbi, Efendi, and N. Sofyan, *Progr. Phys. Met.*, **26**, No. 1: 64 (2025).
31. V. A. Tatarenko, T. M. Radchenko, A. Yu. Naumuk, and B. M. Mordyuk, *Progr. Phys. Met.*, **26**, No. 1: 3 (2025).
32. R. I. Furunzhiev, *Komp'yuternyye Tekhnologii i Ikh Primenenie* [Computer Technology and Its Application] (Minsk: Vysshaya Shkola: 1985) (in Russian).
33. A. A. Turchanin, I. A. Tomilin, and M. A. Turchanin, *Abstracts of 10th International Conference on Liquid and Amorphous Metals (LAM-10) (30 August–4 September, 1998, Germany, Dortmund)*.
34. M. A. Turchanin and I. V. Nikolaenko, *J. Alloys and Comp.*, **236**, Iss. 1–2: 236 (1996).
35. O. V. Oliinyk and V. A. Tatarenko, *Usp. Fiz. Met.*, **13**, No. 4: 417 (2012).
36. M. A. Turchanin and I. V. Nikolaenko, *J. Alloys Comp.*, **235**, Iss. 1: 128 (1996).
37. N. M. Bilyavyna, V. Z. Turkevych, D. A. Stratiichuk, A. M. Kuryliuk, and O. I. Nakonechna, *Progr. Phys. Met.*, **25**, No. 4: 661 (2024).
38. V. A. Dekhtyarenko, T. V. Pryadko, T. P. Vladimirova, C. V. Maksymova, O. M. Semyrga, and V. I. Bondarchuk, *Progr. Phys. Met.*, **25**, No. 4: 765 (2024).
39. O. V. Oliinyk and V. A. Tatarenko, *Usp. Fiz. Met.*, **19**, No. 2: 152 (2018).